

A NUMERICAL HEAT TRANSFER STUDY FOR FULL CHARGING AND DISCHARGING OPERATIONS OF ICE-ON-PIPE STORAGE TANKS

Cleyton Senior Stampa, cleyton@metal.eeimvr.uff.br

UFF, Universidade Federal Fluminense, Av. dos Trabalhadores 420, Volta Redonda, RJ, Brazil, 27255-125

Angela Ourivio Nieckele, nieckele@mec.puc-rio.br

Department of Mechanical Engineering, PUC/Rio, 22453-900, Rio de Janeiro, RJ, Brasil

Abstract. *The present work is concerned with the processes of charging (icing) and discharging (ice melting) occurring into area-constrained ice-on-pipe storage tanks. It consists of an investigation to predict the heat transfer between one typical internal tube settled within the tank and the phase change material (PCM) that surrounds it. The study considers a typical operational condition of such devices, from which the flow and temperature fields are analyzed concerning thermal effectiveness. To do so, natural convection of water near its density maximum is solved in a cell of the storage tank, represented by a vertical annulus. The inner vertical wall represents one of the tubes packed into a typical storage tank, while the outer vertical wall represents the maximum thickness of both liquid or ice layers formed around the tube, which corresponds to the contact of them with the respective layers of the neighbor tubes, depending on the current process. Regarding the annulus, the top and bottom walls, as well as the outer vertical one were considered thermally insulated. Besides, the tank is assumed to be vertically positioned, as well as their internal tubes through which the secondary fluid flows. The present work investigates the influence in the heat transfer at the inner wall due to the process of total freezing followed by total melting of the PCM (water) in contrast to these partial processes. An overview of these processes is analyzed through streamlines and isotherms, for specific instants of the physical processes. Further, a heat transfer analysis for the total charging and discharging stages are presented.*

Keywords: *Energy Storage Tanks, Annular cavity, Natural convection*

1. INTRODUCTION

In this work a numerical study of heat transfer and buoyancy-driven flow structure is presented, by considering natural convection of water near its density maximum (near 4°C, at sea level). The investigation has been conducted in a vertical annular cavity. Past studies have been demonstrated that the inversion phenomenon of cold water and the annulus curvature affect drastically the flow field and the thermal exchange (Lin and Nansteel, 1987). Other works on cold water-filled vertical annular enclosures, submitted to a mixed boundary condition of constant heat flux on the inner wall (Ho and Lin, 1990), revealed for an aspect ratio of 8 the appearance of a multi-cellular flow structure with a wavy maximum density contour at the Rayleigh number of 10^5 . Nevertheless, those works were concerned to steady-state natural convection. It is quite known that the inversion phenomenon of cold water leads to complex flow structure and heat transfer patterns. In this sense, the shape and the formation or destruction velocity of the ice layer along the inner wall are functions of the velocity and temperature fields in the liquid region, which depend on the initial and boundary conditions considered.

Cylindrical geometry is of great importance in the engineering field and, phase-change processes around a cylinder or inside cylindrical cavities are of particular interest in thermal storage devices, mainly concerning the latent thermal energy storage type (LTES). This latter has an important economic aspect due to the advantage of the large heat storage capacity per unit of volume. During the past decade, the use of multiple phase change materials (PCMs) in LTES systems was proposed by several authors to increase the charging and discharging rates of the units, among them (Wang *et al.*, 1999, 2001). Thus, these systems have been widely used in solar energy utilization, industrial waste heat recovery and electrical power load shifting application in recent years (Fath, 1998; Hasnain, 1998; Zalba, *et al.*, 2003; Farid, *et al.*, 2004). The present work deals with this latest application, but using water as the PCM and is intended to contribute with basic information for the design improvement of LTES systems.

Water has been usually adopted as the PCM in typical fusion latent heat storage systems based on indirect, area-constrained, ice-on-pipe storage tanks. LTES for space cooling is an option to reduce electric costs by shifting chilling processes to off-peak times. Thus, heat is removed from the PCM during off-peak times and then passed through a heat exchanger to remove heat from a building in place of chiller operation. In this case, chilled water leaving the chiller passes through a large number of tubes in the tank that transfer the heat from the storage medium (ice/water) to the transport fluid (brine solution) providing a large surface area per unit of storage. For the charging period, cold brine circulates through the tubes and ice is formed on the outside of the tubes, which is melted during the discharging period by a hot brine flow.

The main goal of the researches with respect to these heat storage systems has been the determination of the higher capacity of energy accumulation per unit volume, associated with the thermal conductivity of the phase change material. Performance studies concerning energy storage systems have been the target of many works during the years (Cabeza *et al.*, 2002; Ismail and Silva, 2003; Ismail *et al.*, 2003; Oda *et al.*, 2004; Kayansayan and Acar, 2006; Elsayed,

2007). Several studies of natural convection in vertical annular cavity, considering the water density inversion phenomenon have been presented by Stampa *et al.* (2002, 2003, 2004, 2006). In one of these studies, Stampa *et al.* (2003) investigated the influence in the freezing process of the aspect ratio and radius ratio of the cavity, aiming an increase in the superficial heat transfer area. Natural convection parameters, such as Grashof and Stefan numbers, were also varied, while keeping the other ones fixed. This study showed that the increase of the superficial heat transfer area must be enforced by considering the combined effects of the aspect and radius ratio. In order to continue the performance analysis of ice storage systems, the present work investigates how the radius ratio affects quantitatively the performance of such thermal storage devices in case of full charging and discharging processes. A vertical annular cavity is used as a physical model in order to represent the heat transfer between the brine flowing inside one tube and the water (PCM) that surrounds it suffering solid-liquid phase change. To determine the amount of formed or melted ice, as well as the sensible and latent energy involved in the two processes, the transient heat transfer problem in a water-filled vertical annulus was numerically analyzed with the finite volume method.

2. MATHEMATICAL MODEL

The storage tank is considered as being vertically positioned, as well as their internal tubes through which the secondary fluid (brine) flows. In order to analyze the heat transfer between the PCM and one internal tube during the ice layer growth around it (charging) or during its melting (discharging), a vertical annular cavity was selected as the physical model (Fig. 1). The annular cavity height is L and annular gap is W , being R_{in} the inner radius. The inner vertical wall can represent one of the tubes packed into a typical storage tank, while the outer vertical wall represents the thickness of formed ice around the tube.

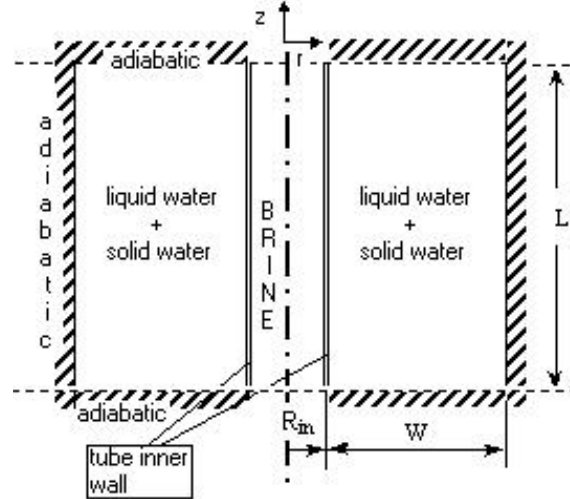


Fig. 1: Physical domain considered

The cavity is filled with water as the PCM, whose melt temperature is $T_m = 0^\circ\text{C}$. Initially, all the system has its temperature settled in a specific value T_{in} , which is superior to T_m for the charging or inferior to it for the discharging process. The boundary conditions are considered as adiabatic at the top and bottom of the cavity, as well as at the external wall. In the beginning of the full charging and discharging processes, it is imposed at the inner wall of the cavity a uniform temperature T_C lower than T_m for the charging process, and T_H greater than T_m in case of the discharging process.

The governing equations are simplified based on the following assumptions: the flow is considered laminar, incompressible, and the PCM is a Newtonian fluid. The physical properties are constant except for the liquid density in the buoyancy term, i. e., this PCM is a Boussinesq liquid. The values estimated for the radius ratios are assumed to be sufficient small, so that the buoyancy-driven flow may be considered axi-symmetric (McFadden *et al.*, 1984). Therefore, due to the angular symmetry, the flow is considered two-dimensional. The conservation equations which govern the process described above are conservation of mass and momentum for the liquid and energy for both solid and liquid phases, which can be express as:

$$\mathbf{div}(\rho_{\ell,ref} \mathbf{U}) = 0 \quad ; \quad \frac{\partial(\rho_{\ell,ref} \mathbf{U})}{\partial t} + \mathbf{div}(\rho_{\ell,ref} \mathbf{U} \mathbf{U}) = \mathbf{div}(\mu_{\ell} \mathbf{grad} \mathbf{U}) - \mathbf{grad} P + \rho_{\ell} \mathbf{g} \quad (1)$$

$$\frac{\partial[(\rho_{\ell,ref} c_{p\ell} \varepsilon + \rho_s c_{ps} (1-\varepsilon)) T]}{\partial t} + \mathbf{div}(\rho_{\ell,ref} \varepsilon \mathbf{U} c_{p\ell} T) = \mathbf{div}[(k_{\ell} \varepsilon + k_s (1-\varepsilon)) \mathbf{grad} T] - \frac{\partial(\rho_{\ell,ref} \varepsilon \Delta h_{lat})}{\partial t} \quad (2)$$

where ρ is the specific mass and μ the absolute viscosity. The subscripts ℓ and s correspond to the liquid and solid properties of PCM. \mathbf{U} is the velocity vector, p is the pressure, \mathbf{g} is the gravitational acceleration vector. The thermo-physical properties of the PCM for the liquid ℓ and solid s phases, expressed by k e cp , are thermal conductivity and specific heat at constant pressure, respectively. T is the temperature of the material and t is the time. Δh_{lat} is the latent heat of fusion and, ε is the volume fraction, which is defined as

$$\varepsilon = \nabla_{\ell} / \nabla \quad (3)$$

where ∇_{ℓ} and ∇ are the liquid volume and the total volume, respectively.

The last term on the right-hand side of Eq. (2) is different from zero only in the regions where the change of phase occurs. The volume fraction ε is equal to one where the PCM is in the liquid phase, and it is set to zero at the regions where the temperature reaches the melting temperature T_m . According to the assumption associated with the buoyancy term, in the third term on the right-hand side of Eq. (1), the following density-temperature relationship of water, proposed by Gebhart *et al.* (1977), was adopted for the liquid density

$$\rho_{\ell} = \rho_{\ell, \text{max}} \left[1 - \text{rsp} |T - T_{\text{max}}|^b \right] \quad (4)$$

where $\rho_{\ell, \text{max}} = 999.972 \text{ kg/m}^3$, $\text{rsp} = 9.297 \times 10^{-6} (\text{°K})^{-b}$, $T_{\text{max}} = 4.029 \text{ °C}$ and $b = 1.895$. This relationship takes into account the nature of the inversion-density in the water.

The boundary conditions associated to these equations are no slip condition at all walls and adiabatic top, bottom and outer wall with constant inner wall temperature, as can be described as

$$\text{for } z=0 \text{ and } z=L ; R_{\text{in}} \leq r \leq (R_{\text{in}} + W) \Rightarrow \partial T / \partial z = 0 \quad (5)$$

$$\text{for } r = (R_{\text{in}} + W) ; 0 \leq z \leq L \Rightarrow \partial T / \partial r = 0 \quad (6)$$

$$\text{for } r = R_{\text{in}} ; 0 \leq z \leq L \Rightarrow T = T_c \text{ or } T = T_H \quad (7)$$

The following dimensionless variables were considered in this mathematical model,

$$U^* = \frac{\rho_{\ell, \text{max}} U W}{\mu_{\ell}} ; \quad \theta = \frac{T - T_m}{T_{\text{in}} - T_m} ; \quad P = \frac{p^* \rho_{\ell, \text{max}}}{(\mu_{\ell} / W)^2} ; \quad Z = \frac{z}{W} ; \quad R = \frac{r}{W} ; \quad \text{Fo} = \frac{\mu_{\ell} t}{\rho_{\ell, \text{max}} W^2} \quad (8)$$

where $p^* = p + \rho_{\ell, \text{max}} g y$. The properties dimensionless parameters that govern the problem can be identified as

$$\rho^* = \frac{\rho_s}{\rho_{\ell, \text{max}}} ; \quad k^* = \frac{k_s}{k_{\ell}} ; \quad cp^* = \frac{cp_s}{cp_{\ell}} ; \quad \text{Pr} = \frac{\mu_{\ell} cp_{\ell}}{k_{\ell}} ; \quad \Phi_m = \frac{T_m}{|T_{\text{in}} - T_m|} ; \quad \Phi_{\text{max}} = \frac{T_{\text{max}}}{|T_{\text{in}} - T_m|} \quad (9)$$

and the geometric dimensionless parameters as

$$\text{RR} = \frac{R_{\text{in}} + W}{R_{\text{in}}} = 1 + \frac{W}{R_{\text{in}}} ; \quad \text{AR} = \frac{L}{W} ; \quad V^* = \frac{\nabla}{\pi W^3} = \left[\frac{\text{RR} + 1}{\text{RR} - 1} \right] \text{AR} \quad (10)$$

where Pr is the Prandtl number, RR the radius ratio, AR the aspect ratio and ∇ is the maximum ice-storage volume, being V^* its dimensionless value. The physical dimensionless parameters are the Grashof number, Gr , and the Stefan number, Ste , besides a sub-cooling parameter, θ_c , all defined by

$$\text{Gr}_L = \frac{\rho_{\ell, \text{max}} g \text{rsp} |T_{\text{in}} - T_m|^b L^3}{\mu_{\ell}^2 / \rho_{\ell, \text{max}}} ; \quad \text{Ste}_{\ell} = \frac{cp_{\ell} |T_{\text{in}} - T_m|}{\Delta h_{\text{lat}}} ; \quad \theta_c = \frac{T_c - T_m}{T_{\text{in}} - T_m} ; \quad \text{Ste}_s = cp^* |\theta_c| \text{Ste}_{\ell} \quad (11)$$

Since the present work concerns the solid-liquid phase change of water, the water/ice properties were kept constant and are shown in Tab. 1.

Table 1: Water/Ice Properties.

PROPERTIES	$\rho_{\text{REF}} = \rho_{\text{L,MAX}}$ (kg/m ³)	cp (J/kg K)	k (W/m ² K)	μ (kg/m s)	Δh_{lat} (J/kg)
WATER	999.97	4200	0.602	0.001203	333600
ICE	999.97	2060	2.3	—	—

3. NUMERICAL METHOD AND ALGORITHM

To solve the set of coupled Eqs. (1) to (2), the finite volume method (Patankar, 1980), has been employed. The convective and diffusive fluxes that cross all faces of each control volume were handled by the Power Law scheme. A fully-implicit time marching technique was considered and the solution method used for the system of linear algebraic equations was the TriDiagonal-Matrix Algorithm-Line-by-Line solver with a Block Correction method. To solve the pressure-velocity coupling, the Semi-Implicit Method for Pressure-Linked Equations was employed (Patankar, 1980).

A fixed and regular grid was adopted on the physical domain with 280×280 nodal points, with a time step of 1 s. These parameters were determined by a grid test; where different mesh sizes and the time step were tested so that heat flux variations inferior to 1% were observed. Solutions were considered converged at a particular time step if the mass and energy residues were inferior to 10^{-6} for at least eight consecutive iterations

4. RESULTS AND DISCUSSION

The present study is concerned with natural convection flow in a water-filled vertical annular cavity, considering the processes of full charging (ice making) and full discharging (ice melting). Numerical simulations were undertaken to study the axi-symmetric transient heat transfer problem. Due to the density inversion phenomenon, when water is cooled near 4°C, a multi-cellular flow patterns can appear within the liquid phase. This regime affects significantly the heat transfer between the PCM and the secondary fluid (brine), which flows inside the tube. The cavity geometric parameters also play a significant role in the thermal exchanges. Therefore, at the present work, the influence of the inner radius R_{in} is analyzed, while keeping the same gap W and height L , by comparing the superficial heat transfer at the inner wall with the thermal energy stored within the annulus.

In the present work, the dimensionless properties parameters, shown in Tab. 2, were kept constant. The numerical simulations were divided into three cases, as shown in Tab. 3, in which different values of RR were adopted while maintaining the aspect ratio AR constant. However, with the RR variation, it was not possible to keep the dimensionless volume V^* constant. The charging and discharging processes were studied for the three cases. Table 4 shows the values of the initial temperature T_{in} and inner wall temperature T_{c} adopted for the charging and discharging processes, while Tab. 5 presents the corresponding constant values of the dimensionless physical parameters.

Table 2. Dimensionless Properties Parameters

ρ^*	k^*	cp^*	Pr
1	3.82	0.49	8.4

Table 3. Geometric Parameters

PARAMETER	CASE 1	CASE 2	CASE 3
W (m)	0.044.8	0.0448	0.0448
L (m)	0.1284	0.1284	0.1284
R_{in} (m)	6.35×10^{-3}	9.525×10^{-3}	12.7×10^{-3}
AR	2.87	2.87	2.87
RR	8.06	5.70	4.53
V^*	3.67	4.08	4.48

Table 4. Initial and boundary temperatures

PARAMETER	MELTING	FREEZING
T_{in} (°C)	-6	+6
T_{c} (°C)	+6	-6

Table 5. Dimensionless Physical Parameters

θ_c	Gr_L	Ste_ℓ	Ste_s	Φ_{max}	Φ_m
-1	3.98×10^6	0.075	0.037	46.2	45.5

The increase of the inner cavity radius (smaller RR) yields to larger cavity volumes, as well as maximum amount of formed ice, $m_{\text{sol(ice),max}}$ leading to greater total times to completely freeze the water and completely melt the ice confined within the region. These value are shown in Tables 6 and 7 for all cases.

The sensible and latent energy stored within the annular region, during the transient processes of charging (freezing) and discharging (melting), were dimensionlized by the maximum possible values of sensible energy ($E_{\text{sen,max}}$) and latent energy ($E_{\text{lat,max}}$) removed as

Freezing:

$$E_{\text{sen}} = \frac{\int_{\forall_{\ell}} \rho_{\ell, \text{max}} \text{cp}_{\ell} (T_{\text{in}} - T) d\forall + \int_{\forall_s} \rho_s \text{cp}_s (T_{\text{m}} - T) d\forall}{E_{\text{sen, max}}} ; E_{\text{sen, max}} = \rho_{\ell, \text{max}} \forall \text{cp}_{\ell} (T_{\text{in}} - T_{\text{m}}) + \rho_s \forall \text{cp}_s (T_{\text{m}} - T_{\text{c}}) \quad (12)$$

Melting:

$$E_{\text{sen}} = \frac{\int_{\forall_{\ell}} \rho_{\ell, \text{max}} \text{cp}_{\ell} (T_{\text{m}} - T) d\forall + \int_{\forall_s} \rho_s \text{cp}_s (T_{\text{in}} - T) d\forall}{E_{\text{sen, max}}} ; E_{\text{sen, max}} = \rho_{\ell, \text{max}} \forall \text{cp}_{\ell} (T_{\text{c}} - T_{\text{m}}) + \rho_s \forall \text{cp}_s (T_{\text{m}} - T_{\text{in}}) \quad (13)$$

Freezing and Melting:

$$E_{\text{lat}} = \frac{\int_{\forall_{\ell, 0^{\circ}\text{C}}} \rho_{\ell, \text{max}} \Delta h_{\text{lat}} d\forall}{E_{\text{lat, max}}} ; E_{\text{lat, max}} = \rho_{\ell, \text{max}} \forall \Delta h_{\text{lat}} \quad (14)$$

where $\forall_{\ell, 0^{\circ}\text{C}}$ represents a control volume, whose temperature has reached 0°C .

The average heat flux on the inner wall of the cavity can be found through the expression given by:

$$\bar{q} = \frac{1}{L} \int_0^L q dz \quad ; \quad q = -k_s \left. \frac{\partial T}{\partial r} \right|_{\text{inner wall}} \quad (15)$$

where q is the local heat flux on the inner wall of the cavity. The average heat flux, \bar{q} , was written in a dimensionless form by

$$q^* = \frac{\bar{q}}{k_{\ell} (T_{\text{max}} - T_{\text{m}}) / W} \quad (16)$$

Further, the mass fraction of ice, f_{ice} , is defined as a function of the variable mass, m , given by:

$$f_{\text{ice}} = \frac{m_{\text{ice}}}{m_{\text{tot}}} = \frac{m_{\text{ice}}}{\rho_{\ell, \text{max}} \forall} = \frac{m_{\text{sol}}}{m_{\text{sol, max}}} \quad (17)$$

The maximum sensible energy and maximum latent energy as well as the maximum dimensionless heat flux at the inner wall of the annulus, are in Table 6 and 7, for the freezing and melting processes, respectively.

Table 6. Maximum dimensionless freezing time and heat flux at the inner wall.

Table 7. Maximum dimensionless melting time and heat flux at the inner wall.

FREEZING	CASE 1 RR=8.06	CASE 2 RR=5.70	CASE 3 RR=4.53
Fo_{max}	21.85	19.58	17.96
$m_{\text{sol(ice),max}}$ (kg)	1.045	1.154	1.269
$E_{\text{sen,max}}$ (W)	6,212	6,897	7,583
$E_{\text{lat,max}}$ (W)	55,169	61,262	67,354
q_{max}^*	107,827	96,129	95,691

MELTING	CASE 1 RR=8.06	CASE 2 RR=5.70	CASE 3 RR=4.53
Fo_{max}	35.787	30.666	27.4618
$m_{\text{sol(ice),max}}$ (kg)	1.045	1.154	1.269
$E_{\text{sen,max}}$ (W)	6,212	6,897	7,583
$E_{\text{lat,max}}$ (W)	55,169	61,262	67,354
q_{max}^*	53,959	53,556	53,422

An overview regarding the freezing process is presented in Figs. 2 through 4, where streamlines and isotherms depict the flow pattern and temperature distribution at each time step mentioned before, for the cases 1, 2 and 3. At each figure, the streamlines are presented on the left side and the isotherms in the right side. Case 2 was selected as a

reference case for the desired comparisons, from which the RR parameter was reduced (Case 3) or increased (Case 1). In the streamline pictures the positive signal for the stream function values indicates a counter-clockwise rotation sense.

Due to the different total melting or freezing time, the dimensionless Fourier time, was normalized by the corresponding maximum Fourier time, shown in Table 4 and 5. The comparison among the three cases was performed, maintaining the normalized time equal to 25%, 50% and 75% of the total dimensionless time for which any process can be considered complete, i. e., the maximum time Fo_{max} .

Analyzing the streamlines for 25% of Fo_{max} , it can be seen that for all cases there is a big counter-clockwise cell in which cold fluid flow occurs upstream adjacent to the solid-liquid interface. The average size of this convective cell increases together with higher values of RR. One also verifies for all cases, the presence of a smaller clockwise rotating cell at the top of the cavity which is separated from the cell mentioned before by a maximum density contour, as it can be seen in the isotherm graphics. This latter cell rotates due to friction effects between these two cells.

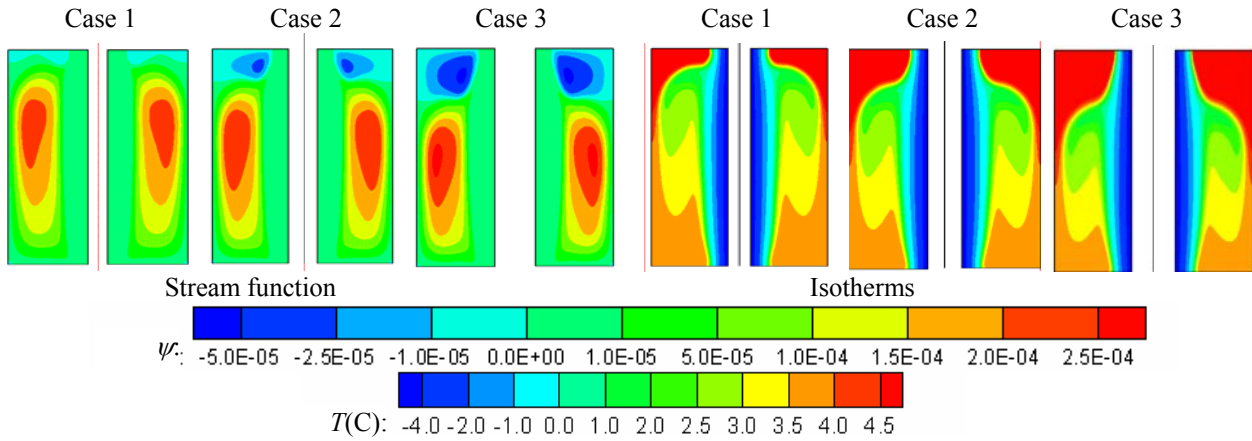


Figure 2. Stream function ψ and isotherms T for 25% of the complete freezing time Fo_{max}

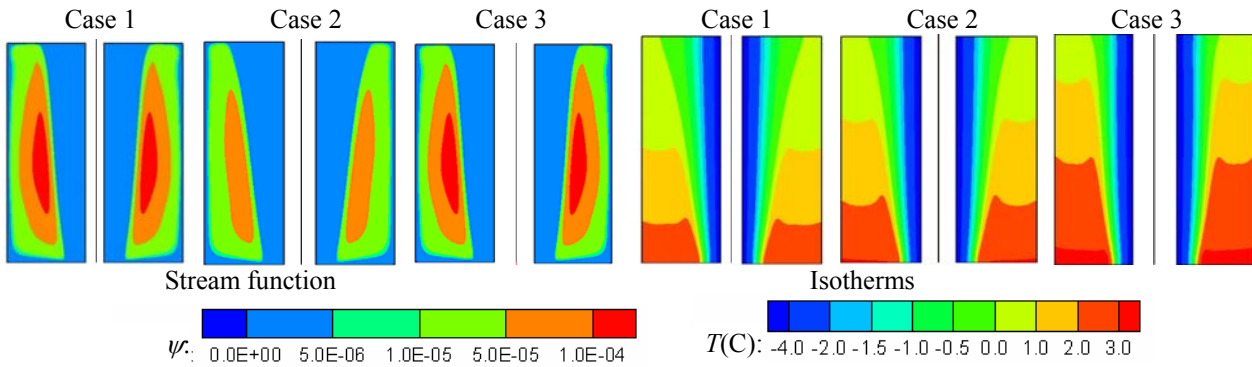


Figure 3. Stream function ψ and isotherms T for 50% of the complete freezing time Fo_{max}

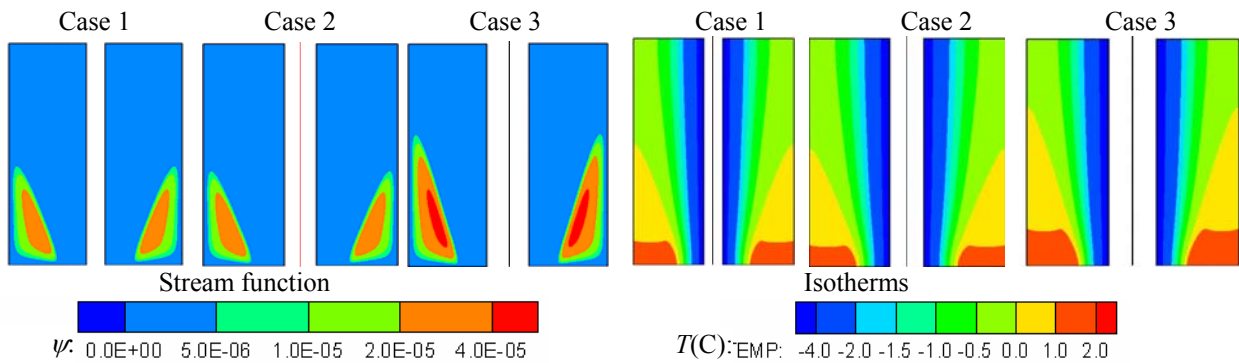


Figure 4. Stream function ψ and isotherms T for 75% of the complete freezing time of Fo_{max}

For the time step 50% of Fo_{max} , the counter-clockwise cell is unique inside the liquid region for all the cases. As can be seen in the isotherm graphics, higher temperatures predominate at the bottom of the cavity, leading to thin ice layers

at that region. This description does not change for later times, and one notes a global temperature decay that diminishes the global drive force of the remaining convective cell, but different intensities are found among the three cases. Some consequences of the above mentioned can be highlighted such as the slope of the solid-liquid interface, which is negative for all cases due to the hottest region at the bottom of the cavity, as it can be seen in Fig. 3 and Fig. 4, which corresponds to 75 % of the total freezing time.

Figures 5 through 7 present the same physical information described in Figs. 2 though 4, but now for the melting process.

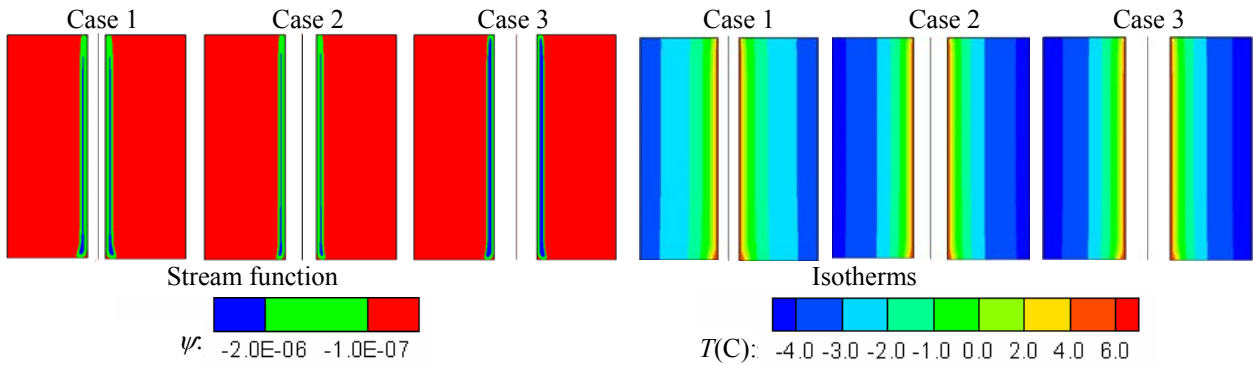


Figure 5. Stream function ψ and isotherms T for 25% of the complete melting time Fo_{max}

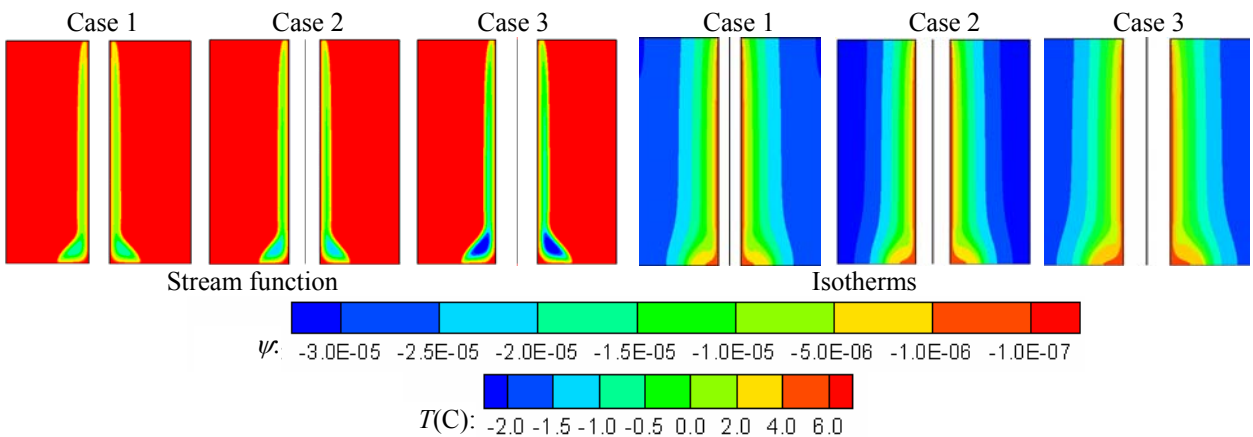


Figure 6. Stream function ψ and isotherms T for 50% of the complete melting time Fo_{max}

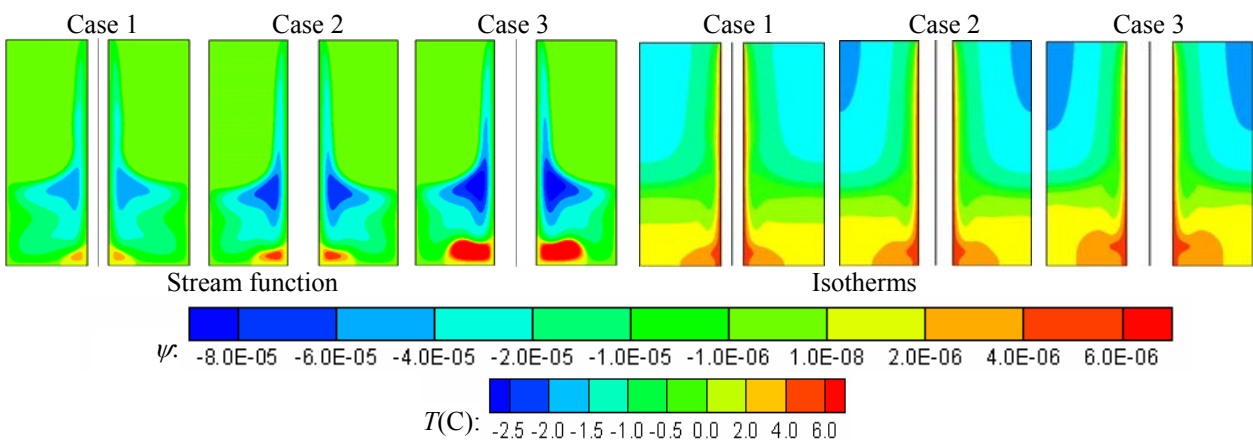


Figure 7. Stream function ψ and isotherms T for 75% of the complete melting time Fo_{max}

Regarding the time step 25% of Fo_{max} , Fig. 5, one verifies the existence of counter-clockwise cells inside the liquid region for all the cases, since this region has a temperature range near T_{max} (4.029 °C). Certainly, the more internal convective cells rotate faster than the other external concentric ones. However, the region of faster cells has the bigger

size for Case 3. Nevertheless, no clockwise rotating cells exist in the liquid region for all cases until this time step. Yet, for 50% of Fo_{max} , as the hotter liquid region becomes bigger, the average movement intensity of the counter-clockwise cells has increased and a faster nucleus appeared at the bottom of the cavity. This nucleus is stronger for Case 3, while is weaker for Case 1. Finally, for 75% of Fo_{max} , one notes the appearance of clockwise cells in the right corner at the bottom of the cavity for all cases, since this region has mean temperature above T_{max} . Once again, these cells are bigger for Case 3 and smaller for Case 1, as a result of the mean temperature in that region for each case.

Besides the flow pattern and temperature distribution analysis presented above for the freezing and melting processes, the present work encompasses other aspects to study natural convection within the water-filled annulus. Thus, it is studied the normalized sensible and latent energy extracted, as well as the mass fraction of ice, all of them as a function of time. It is also investigated the heat flux transient behavior and the heat flux functional behavior related to the sensible and latent energies for the freezing and melting processes.

Starting this analysis by Fig. 8, in which the freezing process is considered, it is noted that the profiles of the three curves are the same. However, for Case 1 a longer dimensionless time is needed to completely form the ice in comparison with Cases 2 and 3. This is a good aspect concerning interception among ice layers of neighbor tubes, which reduces the heat transfer between PCM and brine. On the other hand, the graphics for sensible and latent energies show a slow time response regarding the charging of the cavity, what may be prejudicial in case of rapid demand of energy. Yet, Cases 2 and 3 did not present significant differences in relation to it. Looking back to Figs. 2-4, one verifies that the multi-cellular regime becomes stronger from Case 1 to Case 3, i. e., towards the lowest RR value. So, the results shown in Fig. 8 for the freezing process inform a progressive damage in the thermal exchanges, caused by the presence of a stronger multi-cellular regime together with the RR reduction. Thus, the best heat transfer behavior of Case 1 (highest RR value) described above is confirmed by the results presented in Fig. 9, where the heat flux in all graphics is the highest.

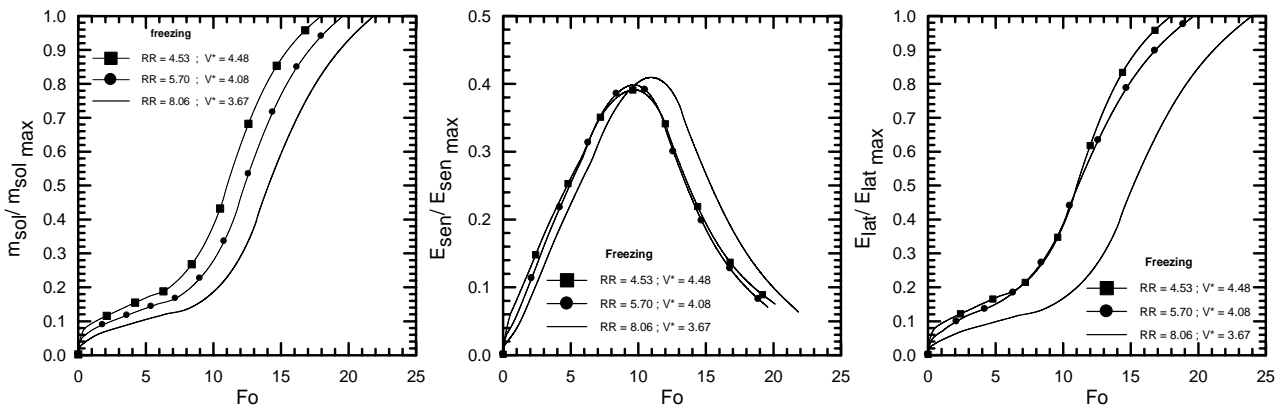


Figure 8. Transient behavior of mass fraction of ice, sensible and latent energies for the freezing process.

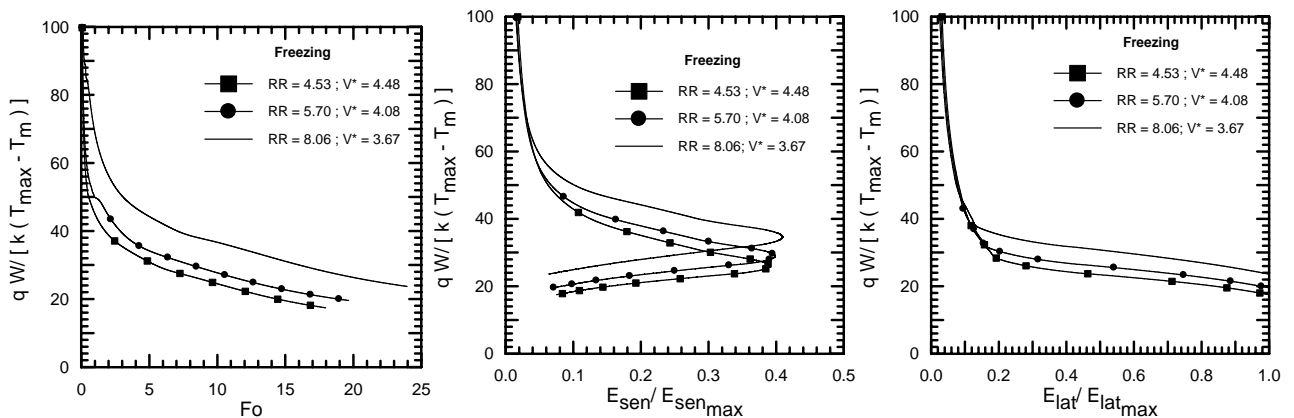


Figure 9. The heat flux transient behavior and the heat flux functional behavior as a function of sensible and latent energies for the freezing process.

Regarding the melting process and looking back to Figs. 4-6, it can be verified from the beginning to time steps near 75% of Fo_{max} that the unique influence in the thermal exchanges was caused by the RR variation, since the multi-cellular regime just appeared for later times. So, the results shown in Figs. 10 and 11 indicated the same best behavior concerning Case 1 as it has occurred in the freezing process, but now for a long period under the RR reduction influence only. However, when the multi-cellular regime appears in the liquid region, as it can be seen in the isotherm graphics of

Figs. 5-7, the damage in the thermal exchanges were reinforced as can it be seen through the change in the slope for the sensible energy and heat flux curves of Figs. 10 and 11.

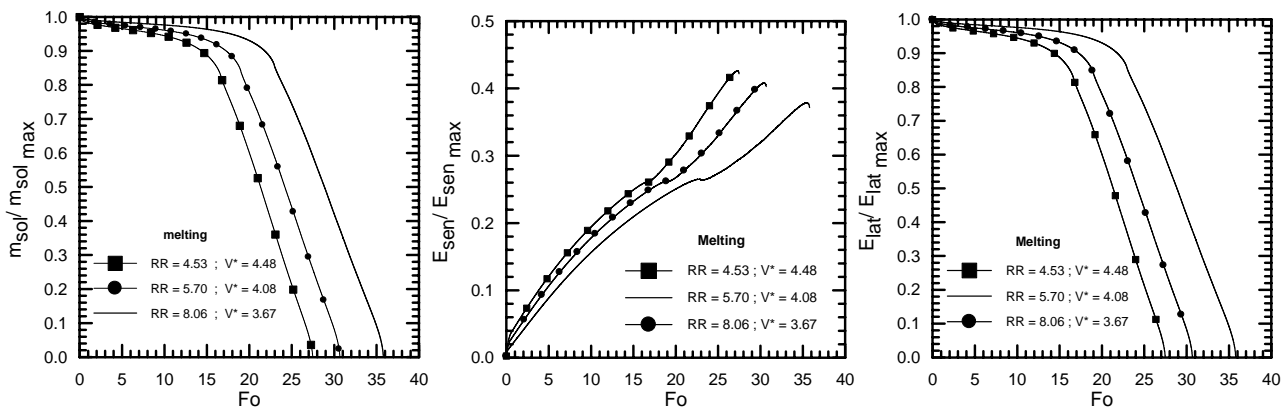


Figure 10. Transient behavior of mass fraction of ice, sensible and latent energies for the melting process.

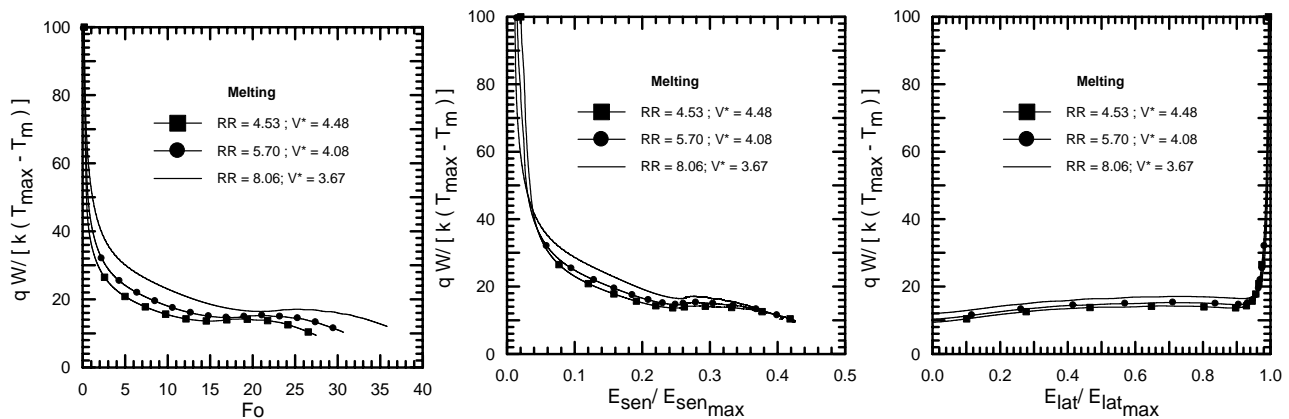


Figure 11. The heat flux transient behavior and the heat flux functional behavior as a function of sensible and latent energies for the melting process.

5. CONCLUSION

The aim of the present study was to contribute with the literature of ice storage systems, more specifically, with the improvement of ice-on-pipe storage tanks design. The task of this work was to investigate the influence of the radius ratio parameter (RR) in the thermal performance of an ice storage tank operating under full charging and discharging regimes, as additional information to be added to other previous studies. So, a numerical study of natural convection occurring in the freezing and melting processes was carried out in a water-filled vertical annulus, used as physical model. In order to represent the heat transfer between the brine flowing inside one tube and the water (PCM) that surrounds it suffering solid-liquid phase change, the present work analyzed the flow patterns and temperature distributions within the cavity, amount of formed or melted ice, sensible and latent energies involved in the two processes and the heat flux on the inner wall of the annulus.

This work considered a variation for the RR parameter within the laminar regime, by diminishing or enlarging it by a factor of 21% and 41%, respectively. It was also kept unchanged the parameters ρ^* , k^* , cp^* , Pr , θ_c , AR , Gr_L , Ste_ℓ , Ste_s , Φ_{max} and Φ_m . The heat transfer analysis was made by using graphics of dimensionless quantities for time, sensible and latent energies and average heat flux on the inner wall of the cavity. In the present study one made use of symmetric initial conditions for the freezing and melting processes in order to observe the moment at which the multi-cellular regime, one of the responsible facts for reducing the thermal exchanges, would appear for each one of the physical processes. This is because the other bad influence in the heat transfer problem, the RR parameter, could be implemented geometrically as it was the proposal of this work. The simulations showed that larger RR (Case 1) seems to be the most favorable geometric arrangement for both full charging and discharging operation conditions. Results within the turbulent regime are still necessary.

6. ACKNOWLEDGEMENTS

The authors acknowledge the support awarded to this research by the Brazilian Research Council, CNPq.

7. REFERENCES

- Cabeza, L. F., Mehling, H., Hiebler, S. and Ziegler, F., 2002, "Heat Transfer Enhancement in Water When Used as PCM in Thermal Energy Storage", *Appl. Thermal Eng.*, Vol. 22, pp. 1141-1151.
- Elsayed, Amr. O., 2007, "Numerical study of ice melting inside rectangular capsule under cyclic temperature of heat transfer fluid", *Energy Conversion and Management*, Vol. 48, pp. 124-130.
- Farid, M.M., Khudhair, A.M., Razack, S.A.K. and Hallaj, S. Al-, 2004, "A review on phase change energy storage: Materials and applications", *Energy Convers. Manage.*, Vol. 45, pp. 1597-1615.
- Fath, H.E.S. 1998, "Technical assessment of solar thermal energy storage technologies", *Renew. Energy*, Vol. 14, No 1, pp. 35-40.
- Gebhart, B., Mollendorf, J. C., 1977, "A New Density Relation for Pure and Saline Water", *Deep Sea Res.*, Vol. 24, pp. 831-848.
- Hasnain, S.M., 1998, "Review on sustainable thermal energy storage technologies, Part I: Heat storage materials and techniques", *Energy Convers. Manage.*, Vol. 39, No 11, pp. 1127-1138.
- Ho, C. J., Lin, Y. H., 1990, "Natural convection of cold water in a vertical annulus with constant heat flux on the inner wall.", *J. Heat Transfer*, Vol. 112, pp. 117-123.
- Ismail, Kamal A. R. and Silva, M. G. E., 2003, "Numerical solution of the phase change problem around a horizontal cylinder in the presence of natural convection in the melt region", *Int. Journal of Heat and Mass Transfer*, Vol. 46, pp.1791-1799.
- Ismail, Kamal A. R., Henriquez, J. R. and Silva, T. M., 2003, "A parametric study on ice formation inside a spherical capsule", *Int. Journal of Thermal Sciences*, Vol. 42, pp.881-887.
- Kayansayan, N. and Acar, M. Ali, 2006, "Ice formation around a finned-tube heat exchanger for cold thermal energy storage", *Int. Journal of Thermal Sciences*, Vol. 45, pp. 405-418.
- Lin, D., Nansteel, N. W., 1987, "Natural convection heat transfer in a vertical annulus containing water near the density maximum.", *J. Heat Transfer*, Vol. 109, pp. 899-905.
- Mcfadden, G. B., Coriell, S. R., Boisvert, R. F. Glicksman, M. E., 1984, "Asymmetric Instabilities in Buoyancy-driven Flow in a Tall Vertical Annulus", *Phys. Fluids*, Vol. 27, pp. 1359-1361.
- Oda, Y., Okada, M., Nakagawa, S., Matsumoto, K. and Kawagoe, T., 2004, "Continuous ice formation in a tube by using water-oil emulsion for dynamic-type ice-making cold thermal energy storage", *Int. Journal of Refrigeration*, Vol. 27, pp. 353-359.
- Patankar, S. V., 1980, "Numerical Heat Transfer and Fluid Flow", Hemisphere Publishing, New York.
- Stampa, C. S., Nieckele, O. A., 2002, "A Numerical Study Of The Growth Of Ice Formation Around A Tube, During The Full Charging Process Of An Indirect, Area-Constrained, Ice-On-Pipe Storage Tank", *The Eighth Joint Thermo physics and Heat Transfer Conference, AIAA-Heat Transfer in Energy Systems*, St Louis, June 24-27.
- Stampa, C. S., Nieckele, O. A. and Braga, S. L., 2003, "A Numerical Parametric Study of the Growth of Ice Formation Around a Vertical Tube, During the Full Charging Process of an Indirect, Area-constrained, Ice-on-pipe Storage Tank", *Summer Heat Transfer Conference-ASME*, Las Vegas, USA
- Stampa, C. S., Nieckele, O. A., 2004, "A Numerical Study Concerning Indirect Ice Storage Tanks", *Proceedings of IMECE 2004 International Mechanical Engineering Congress and RD&D Expo Anaheim, California, USA*, November 13-19, 2004. IMECE2004-60677
- Stampa, C. S., Nieckele, O. A., 2006, "Numerical Analysis Of Indirect Ice Storage Systems Performance", *Thermal Engineering*, Vol. 5 (1), pp.84-89.
- Zalba, B., Marin, J.M., Cabeza, L.F. and Mehling, H., 2003, "Review on thermal energy storage with phase change: materials, heat transfer analysis and applications", *Appl. Therm. Eng.*, Vol. 23, pp. 251-283.
- Wang, J.F., Chen, G.M. and Zheng, F., 1999, "Study on phase change temperature distributions of composite PCMs in thermal energy storage systems", *Int. J. Energy Res.*, Vol. 23, pp. 277-285
- Wang, J.F., Ouyang, Y.X. and Chen, G.M., 2001, "Experimental study on charging processes of a cylindrical heat storage capsule employing multiple-phase-change materials", *Int. J. Energy Res.*, Vol. 25, pp. 439-447

8. RESPONSIBILITY NOTICE

The authors are the only responsible for the printed material included in this paper.